

Special  
Collection

# Near-Infrared Circularly Polarised Luminescence from Helically Extended Chiral *N,N,O,O*-Boron Chelated Dipyrromethenes

Nawaf Algoazy,<sup>[a]</sup> Rebecca G. Clarke,<sup>[a]</sup> Thomas J. Penfold,<sup>[a]</sup> Paul G. Waddell,<sup>[a]</sup> Michael R. Probert,<sup>[a]</sup> Roy Aerts,<sup>[b]</sup> Wouter Herrebout,<sup>[b]</sup> Patrycja Stachelek,<sup>[c]</sup> Robert Pal,<sup>[c]</sup> Michael J. Hall,<sup>\*[a]</sup> and Julian G. Knight<sup>\*[a]</sup>

Synthetically straightforward  $\pi$ -extension of helically chiral *N,N,O,O*-boron chelated borondipyrromethenes (BODIPYs) has been achieved by incorporation of naphthyl rings into the BODIPY 3- and 5-positions. The effect of this extension on the photophysical and chiroptical properties is strongly dependent on the regiochemistry of the naphthyl substituents (**4***exo*, **4***lin*,

**4***endo*). The most helicene-like regioisomer **4***endo* is a near infra-red (NIR) emitter ( $\lambda_{max}^{em} = 751$  nm) with an emission band between 675–875 nm, displaying circularly polarised luminescence (CPL) with a luminescence dissymmetry factor,  $|g_{lum}| = 5.7 \times 10^{-3}$  and CPL brightness,  $B_{CPL} = 27$ , rivalling the best NIR CPL-emitting small organic molecules reported to date.

## Introduction

Circularly polarized luminescence (CPL), the differential emission of left- or right-handed circularly polarized light from a chiral excited state, has potential applications which include imaging displays,<sup>[1]</sup> information encoding and encryption,<sup>[2]</sup> optoelectronic devices,<sup>[3]</sup> asymmetric synthesis,<sup>[4]</sup> and sensing.<sup>[5]</sup> The performance of CPL-active species can be usefully quantified by the luminescence dissymmetry factor (degree of circular polarization),  $g_{lum}$ , which takes values between +2 (100% left-handed) and –2 (100% right-handed) and the CPL-brightness  $B_{CPL}$  which is the product of  $|g_{lum}|/2$ , the absorption extinction coefficient ( $\epsilon$ ), and the luminescence quantum yield ( $\phi$ ).<sup>[6]</sup> CPL-SOMs (small organic molecules) have several attrac-

tive features which result from the power and versatility of synthetic organic chemistry to create structural variations: fine-tuning of absorption and emission wavelengths; introduction of chiral perturbations; control of physical properties such as solubility; functionalization enabling incorporation into materials by control of aggregation, supramolecular chemistry and polymerization.<sup>[7]</sup> Despite the significant advances in designing CPL-SOMs with high values of both  $|g_{lum}|$  and  $B_{CPL}$  at shorter wavelengths, there have been very few reports of effective SOMs capable of CPL emission in the near infra red (NIR, >750 nm) region, which is particularly important for potential applications in bioimaging since this is the wavelength range which displays the maximum depth of penetration in biological tissues.<sup>[8]</sup> Jiang and Wang have reported the spiro-fused terylene dimer **1** which displays emission between 650 and 900 nm with maximum CPL at 701 nm with  $|g_{lum}| = 9 \times 10^{-4}$  and  $B_{CPL} = 11.5$  (Figure 1).<sup>[9]</sup> De la Moya has reported the BINOLated bisaminostyrylBODIPY **2**, emitting CPL from 675 to 850 nm with maximum  $|g_{lum}| = 1.6 \times 10^{-3}$  at 780 nm and  $B_{CPL} = 25$ .<sup>[10]</sup> We have previously reported a series of chiral *N,N,O,O*-boron chelated dipyrromethenes **3** (Figure 1) in which the  $|g_{lum}| = 4.3 \times 10^{-3}$  (637 nm) (**3**, R = *p*-tolyl).<sup>[11]</sup> We proposed that the CPL emission from these BODIPYs might be bathochromically shifted towards the NIR region in a straightforward way by  $\pi$ -extension of the aromatic substituents in the 3- and 5-positions from phenol to naphthols. There are three regioisomeric naphthol derivatives, depending on the position of substitution of the second aryl ring (**4***exo*, **4***lin*, **4***endo*, Scheme 1). In addition to the  $\pi$ -extension, it is also notable that the structure of the **4***endo* isomer more strongly resembles a helicene in comparison to **4***exo* and **4***lin*. Mori and Inoue have nicely demonstrated that, for small helicenes, electric ( $\mu$ ) and magnetic ( $m$ ) transition dipoles become more closely aligned as the number of rings is increased, a feature which contributes to a larger anisotropy ( $g$ ) factor.<sup>[12]</sup> This effect might therefore

[a] N. Algoazy, Dr. R. G. Clarke, Dr. T. J. Penfold, Dr. P. G. Waddell, Dr. M. R. Probert, Dr. M. J. Hall, Dr. J. G. Knight  
Chemistry – School of Natural and Environmental Sciences  
Bedson Building  
Newcastle University  
Newcastle upon Tyne, NE1 7RU (UK)  
E-mail: Michael.Hall@newcastle.ac.uk  
Julian.Knight@newcastle.ac.uk

[b] R. Aerts, Prof. W. Herrebout  
Department of Chemistry  
University of Antwerp  
Groenenborgerlaan 171  
2020 Antwerp (Belgium)

[c] Dr. P. Stachelek, Dr. R. Pal  
Department of Chemistry  
Durham University  
South Road, Durham, DH1 3LE (UK)

Supporting information for this article is available on the WWW under <https://doi.org/10.1002/cptc.202200090>

An invited contribution to a Special Collection on Circularly Polarized Luminescence

© 2022 The Authors. ChemPhotoChem published by Wiley-VCH GmbH. This is an open access article under the terms of the Creative Commons Attribution License, which permits use, distribution and reproduction in any medium, provided the original work is properly cited.

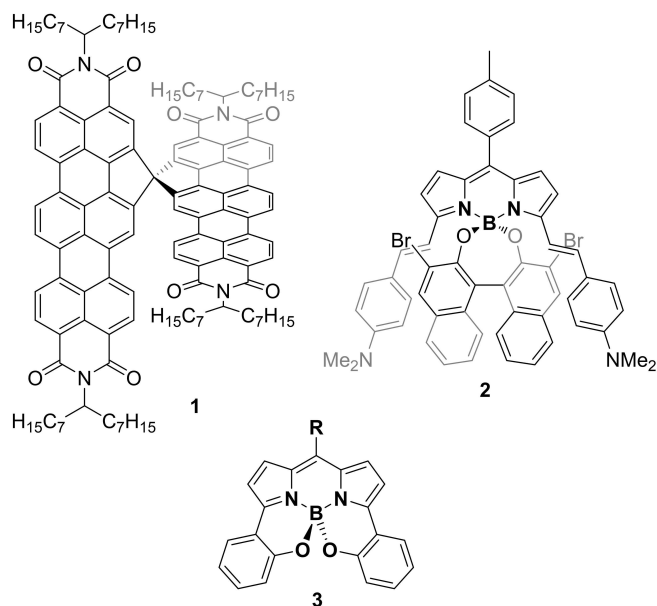


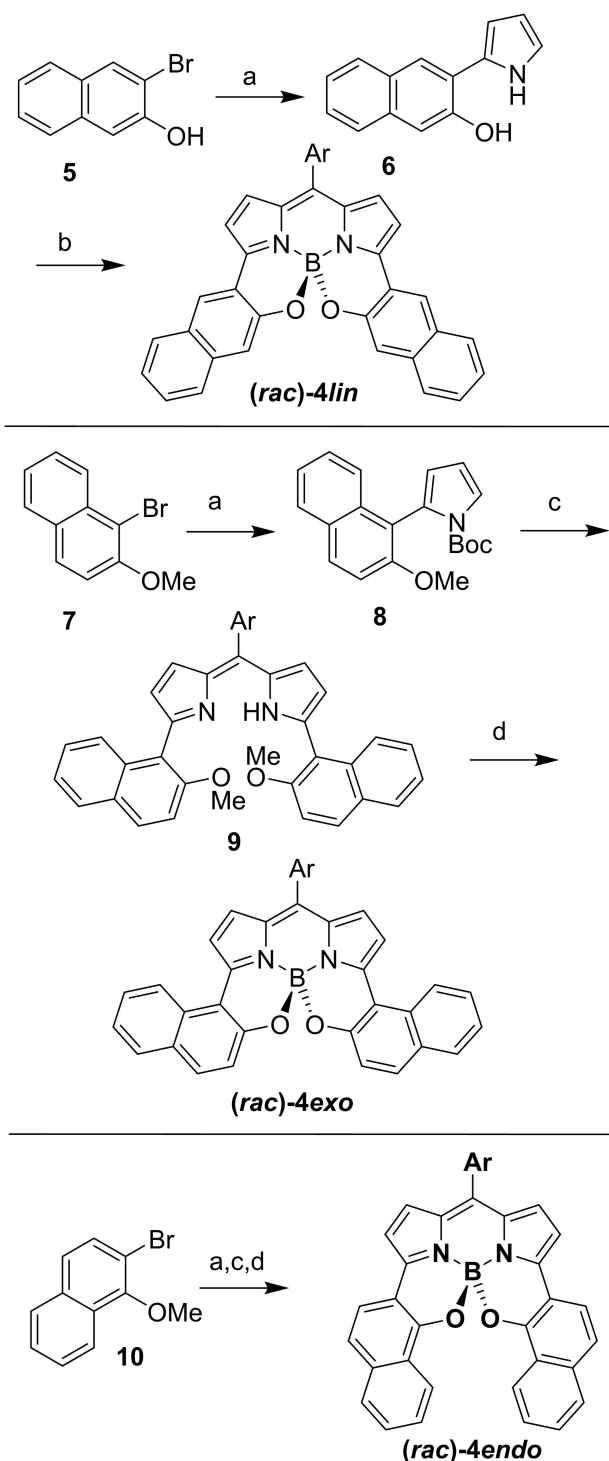
**Figure 1.** Previously reported NIR CPL-SOMs **1**<sup>[9]</sup> and **2**<sup>[10]</sup> and our CPL-active phenol-based chiral *N,N,O,O*-boron chelated dipyrromethene **3** (R = *p*-tolyl).<sup>[11]</sup>

lead to an increased  $|g_{lum}|$  in the case of the **4*endo*** isomer, for which the structure is essentially a hetero[7]helicene. While it is possible to envisage helicene-like BODIPYs in which the pyrrole rings are extended by polyaromatic carbocyclic ring fusion, the synthetic route to such compounds would be vastly more lengthy and complex than the *N,N,O,O*-chelated systems **4**.

The targeted naphthyl-extended *N,N,O,O*-boron chelated compounds **4** also feature replacement of the methyl group of the *para*-tolyl meso substituent of the previously reported **3** with a methyl ester. This modification offers a small additional  $\pi$ -extension but more importantly provides functionality suitable for future elaboration (such as the inclusion of water-solubilising substituents).

## Results and Discussion

The *N,N,O,O*-chelated linearly-extended BODIPY **4*lin*** was prepared via a highly efficient, two-step sequence from 3-bromo-2-naphthol **5** (Scheme 1). Suzuki-Miyaura coupling with *N*-Boc-pyrrole 2-boronic acid proceeded with concomitant Boc-deprotection to give the aryl pyrrole **6** in 84% yield. One pot, acid catalysed condensation with 4-methoxycarbonyl-benzaldehyde, DDQ oxidation and boron chelation by reaction with boron trifluoride in the presence of Hünig's base gave the BODIPY **4*lin*** in 37% yield. In the case of the **4*exo*** and **4*endo*** isomers, this concise route was not viable due to formation of substantial amounts of cyclic carbonate resulting from reaction between the naphthol OH and the pyrrolic Boc protecting group during attempted Suzuki-Miyaura couplings. For these isomers the appropriate bromonaphthol was protected as the corresponding methyl ether (**7** and **10**), necessitating a longer sequence of: Suzuki-Miyaura coupling; thermolytic Boc depro-



**Scheme 1.** Synthesis of regioisomeric naphthol-derived strapped BODIPYs **4*lin***, **4*exo***, **4*endo***. Ar = 4-MeO<sub>2</sub>CC<sub>6</sub>H<sub>4</sub>. a) *N*-BocPyrrole-2-boronic acid, [G3-XPhosPdOMs]<sup>[13]</sup> (3 mol%), K<sub>3</sub>PO<sub>4</sub>, THF/H<sub>2</sub>O, 70 °C, 24 h (**6**, 84%; **8**, 69%; from **10**, 62%); b) 4-MeO<sub>2</sub>CC<sub>6</sub>H<sub>4</sub>CHO, TFA, CH<sub>2</sub>Cl<sub>2</sub>, rt, 3 h; DDQ, rt, 1 h; *i*-Pr<sub>3</sub>NEt, BF<sub>3</sub>·OEt<sub>2</sub>, rt, 6 h (37%); c) 200 °C, 30 min. (from **8**, 89%; route from **10** 67%); 4-MeO<sub>2</sub>CC<sub>6</sub>H<sub>4</sub>CHO, TFA, CH<sub>2</sub>Cl<sub>2</sub>, rt, 3 h; DDQ, rt, 1 h (**9**, 37%; route from **10**, 37%); d) BBr<sub>3</sub>, CH<sub>2</sub>Cl<sub>2</sub>, -78 °C to rt, 5 h (**4*exo***, 78%; **4*endo***, 57%).

tection; aldehyde condensation and DDQ oxidation; and finally a boron tribromide induced tandem demethylation and boron chelation (Scheme 1).

Following the growth of suitable single crystals from racemic samples by slow diffusion of hexane into dichloromethane solution, X-ray crystal structures of all three regioisomeric BODIPYs **4*exo***, **4*lin*** and **4*endo*** were obtained (Figure 2). In each case, it is clear to see that the geometric constraint imposed by chelation of the naphthol to the boron leads to loss of planarity of the central BODIPY core.

The relative angle between the two pyrrole planes, which can be referred to as a ‘twist’, is actually very small and does not vary significantly between the three isomers (Table 1). A

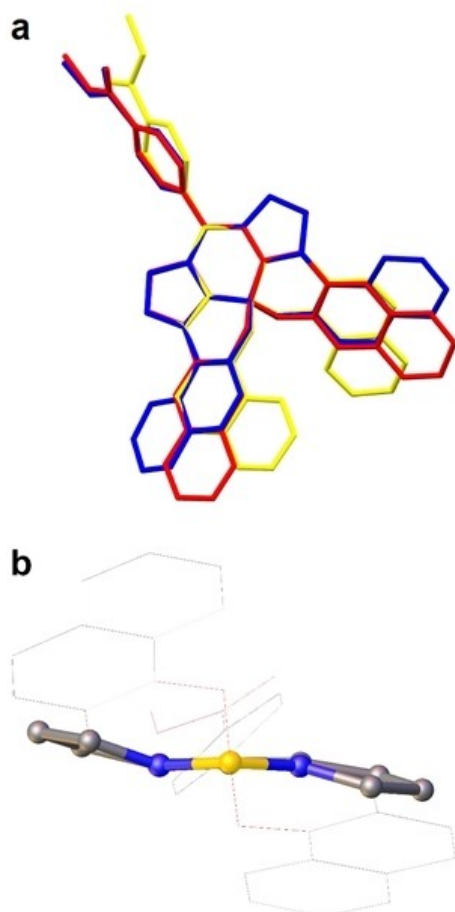


**Figure 2.** (a) Overlay of X-ray crystal structures of: **4*exo*** (blue), **4*lin*** (red), **4*endo*** (yellow), illustrating the closely similar geometry of the three isomers. (b) Perspective view of the BODIPY core of **4*endo***, illustrating the chiral, stepped geometry and the small degree of twist between the pyrrole planes. Hydrogen atoms have been omitted for clarity.

**Table 1.** The conformation of the BODIPY core: selected geometric parameters for **4*exo***, **4*lin***, and **4*endo***.

Compound	Twist <sup>[a]</sup>	Fold-1 <sup>[b]</sup>	Fold-2 <sup>[b]</sup>	RMSD <sup>[c]</sup>
<b>4<i>exo</i></b>	5.7°	13.1°	10.6°	0.093
<b>4<i>lin</i></b>	5.9°	12.4°	14.8°	0.104
<b>4<i>endo</i></b>	6.2°	12.1°	15.7°	0.108

[a] Angle between the two pyrrole planes. [b] Angle between the normals to the planes of the pyrrole and central 6 m ring. [c] Root mean square deviation from the mean for atomic positions of the central 5m–6m–5 m BODIPY tricycle.

more apparent chiral feature of the central BODIPY fluorophore is a pronounced ‘step’ arrangement (Figure 2b) resulting from folding between the pyrroles and the central six-membered boron chelate (fold angles are shown in Table 1). It is notable that the geometry of the tricyclic BODIPY cores of all three isomers are extremely similar and overlay very closely (RMSD  $\approx 0.1$  Å, Table 1). It appears that differences between the photophysical and chiroptical properties of the three isomers are unlikely to arise purely due to such subtle differences in the geometry of the central dipyrromethene ring system.

The UV/Vis absorption spectra of dichloromethane solutions of each of the three regioisomeric naphthol-chelated BODIPYs (Figure 3) show that the long-wavelength absorption maximum of all three isomers is above 600 nm, suggesting extended  $\pi$ -conjugation of the fluorophore (in comparison, the non-naphthyl analogue **3** (R = 4-MeC<sub>6</sub>H<sub>4</sub>) displays<sup>[11]</sup>  $\lambda_{max}^{abs} = 622$  nm and  $\lambda_{max}^{em} = 637$  nm) but do not form a monotonic progression from *exo* to *linear* to *endo*. Both the *exo* and *endo* isomers are

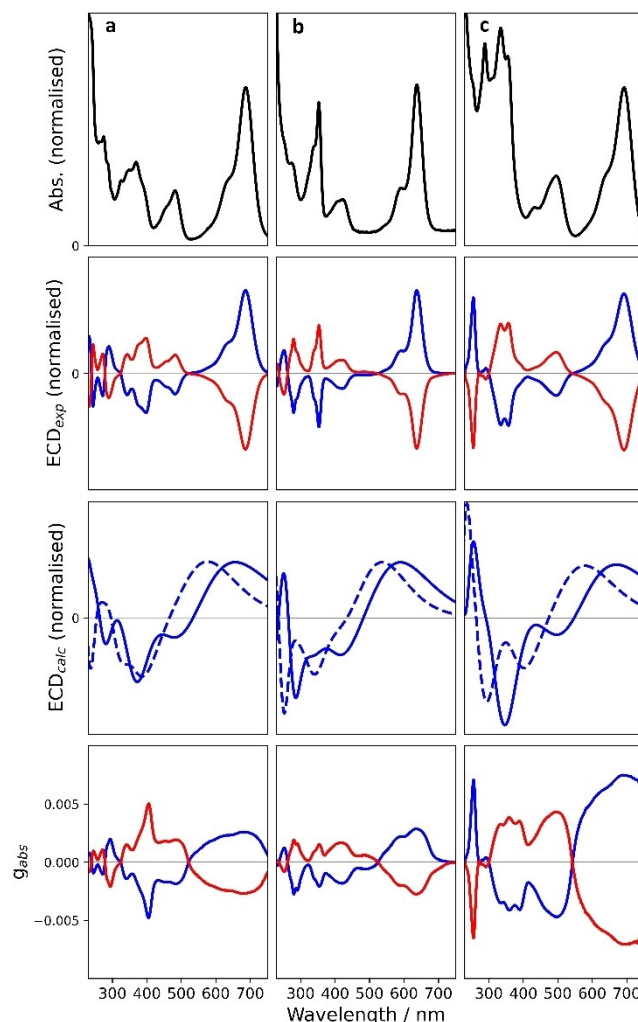


**Figure 3.** Normalised UV/Vis absorption spectra (black) (top) [CH<sub>2</sub>Cl<sub>2</sub>]. Experimental ECD spectra recorded for the *P* (blue) and *M* (red) configurations, (upper middle) [CH<sub>2</sub>Cl<sub>2</sub>]. Calculated ECD spectra computed at the B3LYP/6-311++G(3df, 2pd) (full line) and CAM-B3LYP/6-311++G(3df, 2pd) (dashed line) levels of theory for the *P* configuration (lower middle).  $g_{abs}$  vs wavelength (bottom): **4*exo*** (a), **4*lin*** (b), and **4*endo*** (c).

significantly red-shifted and also display a higher molar extinction coefficient ( $\epsilon$ ) in relation to the *linear* isomer (Table 2). A similar pattern is shown in the emission spectra (Figure 4 and Table 2). The emission maximum of the *exo* and *endo* isomers appear at 741 and 751 nm respectively, very red-shifted in comparison with the *linear* isomer (665 nm). The luminescence quantum yield of the linear isomer ( $\phi_f$ ) is also much lower than the other two isomers (Table 2). It is notable that the emission spectra ( $\lambda^{em}$  675 to 875 nm) for **4*exo*** and **4*endo*** occupy the low-wavelength region of the NIR range.

All three regioisomers could be resolved into single enantiomers by semi-preparative chiral HPLC (see Supporting Information) to enable investigation of their chiroptical properties.

Each of the three enantiomeric pairs displays mirror image electronic circular dichroism (ECD) spectra (Figure 3). To assign the correct configuration ECD spectral calculations were performed using two theoretical levels: B3LYP/6-311++G-

Compound	$\lambda_{max}^{abs}$ [nm] <sup>[a]</sup>	$\epsilon$ [M <sup>-1</sup> cm <sup>-1</sup> ]	$\lambda_{max}^{em}$ [nm] <sup>[b]</sup>	$\phi_f$ <sup>[c]</sup>	$ g_{abs} _{calc}$	$ g_{abs} _{exp}$ <sup>[d]</sup>
<b>4<i>exo</i></b>	687	45 700	741	0.24	$2.00 \times 10^{-3}$	$2.6 \times 10^{-3}$
<b>4<i>lin</i></b>	631	36 400	665	0.02	$2.80 \times 10^{-3}$	$2.8 \times 10^{-3}$
<b>4<i>endo</i></b>	691	67 700	751	0.14	$5.99 \times 10^{-3}$	$7.4 \times 10^{-3}$

[a] In CH<sub>2</sub>Cl<sub>2</sub>. [b] Excitation  $\lambda = 565$  nm. [c] Quantum yield in CH<sub>2</sub>Cl<sub>2</sub> vs. cresyl violet ( $\phi_f = 0.56$ , EtOH).<sup>[16]</sup> [d]  $|g_{abs}|_{exp}$  at the respective  $\lambda_{max}^{abs}$  in CH<sub>2</sub>Cl<sub>2</sub>.

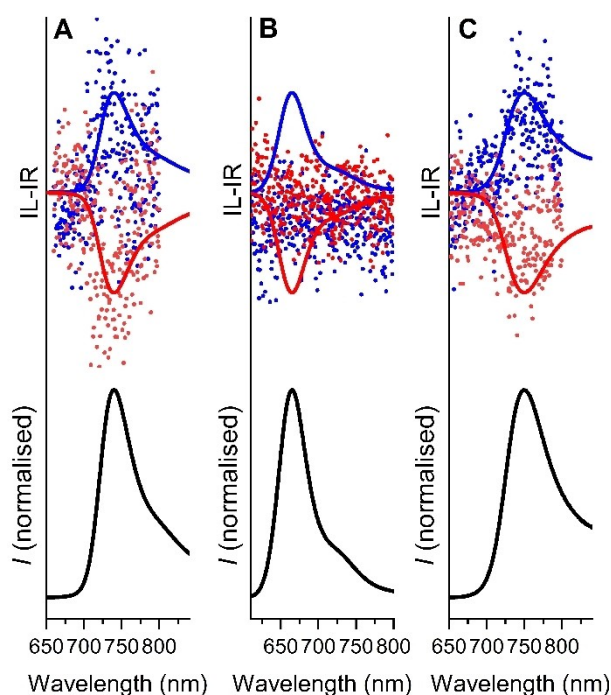


Figure 4. Normalised emission spectra (black) and CPL spectra for *M* (red) and *P* (blue) configurations: **4*exo*** (A,  $\lambda^{ex}$  500 nm), **4*lin*** (B,  $\lambda^{ex}$  590 nm), and **4*endo*** (C,  $\lambda^{ex}$  640 nm) [CH<sub>2</sub>Cl<sub>2</sub>].

(3df,2pd) and CAM-B3LYP/6-311++G(3df,2pd). As observed before, the CAM-B3LYP functional overestimates the excitation energies by about 100 nm.<sup>[14]</sup> The ECD patterns calculated on both theoretical levels are, nevertheless, very similar (considering the mentioned excitation energy shift) and generally compare well with the experiments, apart from the vibrational signatures. The vibrational levels could, in principle, be included in the predictions as presented by Ponce-Vargas *et al.*,<sup>[15]</sup> but are not required for the current chiral centre assignment. The aforementioned relative blue-shift of the long-wavelength transition of the *linear* isomer is reproduced in the spectral calculations. The *P/M* configuration can readily be determined: the *P* configuration is assigned to the enantiomer displaying a positive long-wavelength band for all the three regioisomers (blue ECD spectrum in Figure 3).

The enantiomeric pairs produced mirror-image CPL spectra which align well with the emission spectrum for both the **4*exo*** ( $|g_{lum}| = 1.4 \times 10^{-3}$ ) and **4*endo*** ( $|g_{lum}| = 5.7 \times 10^{-3}$ ) isomers (Figure 4 and Table 3). In contrast, the CPL detected from the **4*lin*** isomer was too weak to enable  $g_{lum}$  measurement (Figure 4b). The **4*endo*** isomer thus represents a NIR CPL emitter with a CPL brightness<sup>[6]</sup> ( $B_{CPL} = \epsilon \times \phi \times g_{lum}/2$ ) = 27 at 751 nm in CH<sub>2</sub>Cl<sub>2</sub>, comparable to the highly optimised BINOLated bis(aminostyryl)-based BODIPY<sup>[10]</sup> **2** ( $B_{CPL} = 25$  at 780 nm in CHCl<sub>3</sub>).

The luminescence dissymmetry factor  $|g_{lum}|$  can be expressed in terms of the electric ( $\mu$ ) and magnetic ( $m$ ) transition dipole moments and the angle between them ( $\theta$ ) [ $g_{lum} = 4|\mu| \cdot |m| \cdot \cos\theta / (|\mu|^2 + |m|^2)$ ]. These values were calculated using CIS(D)<sup>[17]</sup> and def2-TZVP basis set<sup>[18]</sup> as implemented within the ORCA<sup>[19]</sup> quantum chemistry package (the corresponding values of the transition dipole moments and angle for *absorption*, used to calculate  $g_{abs}$ , are shown in the Supporting Information). The effect of the solvent was incorporated by applying a polarizable continuum solvent model using the parameters for dichloromethane (Tables 2 and 3). The calculations are in good agreement with the experimentally observed order of  $|g_{lum}|$  values (Table 3) and predict that the **4*lin*** isomer will have a very low  $|g_{lum}|$  principally due to a magnetic transition dipole moment two orders of magnitude smaller than that of the other two isomers. The higher calculated  $|g_{lum}|$  of the **4*endo*** isomer results both from an angle ( $\theta = 74.6$ ) much further from 90° than that of the **4*exo*** isomer ( $\theta = 82.8$ ) and also a  $\mu : m$  ratio closer to 1 (the value of  $|g_{lum}|$  is maximised when  $|\mu| = |m|$ ).

Table 3. Calculated electric ( $\mu$ ) and magnetic ( $m$ ) transition dipole moments, the angle between them ( $\theta$ ), and  $|g_{lum}|_{calc}$  in comparison with  $|g_{lum}|_{exp}$  for **4*exo***, **4*lin***, and **4*endo***.

Compound	$\mu$ [esu cm]	$m$ [esu cm]	$\theta$ °	$ g_{lum} _{calc}$	$ g_{lum} _{exp}$ <sup>[b]</sup>
<b>4<i>exo</i></b> <sup>[a]</sup>	$7.66 \times 10^{-18}$	$1.15 \times 10^{-20}$	82.8	$7.52 \times 10^{-4}$	$1.4 \times 10^{-3}$
<b>4<i>lin</i></b> <sup>[a]</sup>	$2.48 \times 10^{-18}$	$4.32 \times 10^{-22}$	75.3	$1.70 \times 10^{-4}$	n/a <sup>[c]</sup>
<b>4<i>endo</i></b> <sup>[a]</sup>	$5.78 \times 10^{-18}$	$1.57 \times 10^{-20}$	74.6	$2.99 \times 10^{-3}$	$5.7 \times 10^{-3}$

[a] Excitation  $\lambda$ : **4*exo*** = 500 nm; **4*lin*** = 590 nm; **4*endo*** = 640 nm. [b]  $|g_{lum}|_{exp}$  at the respective  $\lambda_{max}^{em}$  in CH<sub>2</sub>Cl<sub>2</sub>; [c] CPL signal too weak to enable  $g_{lum}$  measurement.

The calculated electronic density difference maps for S1→S0 (Figure 5) indicate that, while for all three regioisomers the transition is localized mainly on the BODIPY core, there is a distinct contribution from both the *meso*-aryl ring and the oxygen chelate rings, including the main naphthyl  $\pi$ -system.

The extremely similar geometries of the BODIPY 'core' observed in the X-ray crystal structures, the significant extension of the HOMO, in particular, over both the BODIPY core and the naphthyl ring systems (see Supporting Information), the strong influence of the naphthyl ring regiochemistry on both the experimental absorption, emission, ECD and CPL spectra and also on the calculated magnitudes and relative direction of the electric and magnetic transition dipoles and contribution of the naphthyl  $\pi$ -system to the electron density difference for the S1→S0 transition all suggest that the effect of the naphthyl group is not simply in effecting a chiral distortion of the main BODIPY core. Nonetheless, the relatively small contribution of the naphthyl  $\pi$ -system to the S1→S0 transition suggests that these systems fall at the borderline between CPL emitters that are intrinsically chiral and those involving chiral perturbation.<sup>[20]</sup>

## Conclusion

Synthetically straightforward  $\pi$ -extension of helically chiral *N,N,O,O*-boron chelated BODIPYs has been achieved by incorporation of naphthyl rings into the BODIPY 3- and 5-positions. The effect of this extension on the photophysical and chiroptical properties is strongly dependent on the regiochemistry of the naphthyl substituents (**4*exo***, **4*lin***, **4*endo***). The most helicene-like regioisomer **4*endo*** is a NIR emitter ( $\lambda_{max}^{em} = 751$  nm) with an emission band between 675–875 nm, displaying CPL with a  $|g_{lum}| = 5.7 \times 10^{-3}$  and  $B_{CPL} = 27$ , rivalling the best NIR CPL-emitting small organic molecules reported to date.<sup>[9–10]</sup> Further structural modification, to introduce water solubility, for example by inclusion of PEGylated or sulfonated substituents is anticipated to be possible via the *meso*-ester group or by substitution at the 2- and 6-positions of the BODIPY core. Additional elaboration to increase the two photon absorption cross-section, for example by additional  $\pi$ -extension of the conjugated system, might make these chiral NIR emitters

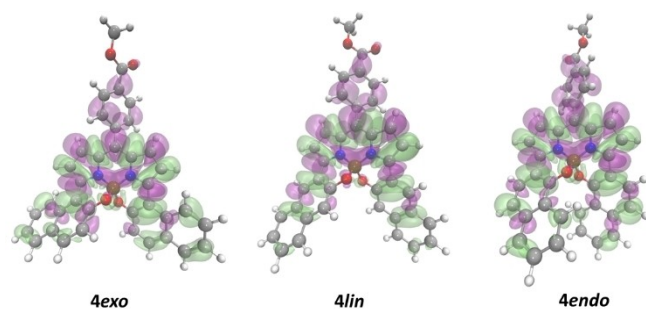


**Figure 5.** Difference of electronic density for the S1→S0 transition at the S1 equilibrium geometry for **4*exo***, **4*lin***, and **4*endo*** (purple: gain in electronic density, lime: loss).

suitable for multiphoton microscopy and cell imaging<sup>[21]</sup> and is the subject of further investigations.

## Experimental Section

Full experimental details and compound characterization data are given in the Supporting Information.

**CCDC deposition numbers:** 2163735 (for **4*exo***), 2163734 (for **4*lin***), 2163736 (for **4*endo***) contain the supplementary crystallographic data for this paper. These data are provided free of charge by the joint Cambridge Crystallographic Data Centre and Fachinformationszentrum Karlsruhe Access Structures service

## Acknowledgements

We thank Newcastle University for financial support of this work. NA thanks the Saudi Arabian Cultural Bureau for financial support in the form of a King Abdullah Scholarship. The University of Antwerp (BOF-NOI) is acknowledged for the pre-doctoral scholarship of RA. The resources and services used in this work were provided by the VSC (Flemish Supercomputer Center), funded by the Research Foundation - Flanders (FWO) and the Flemish Government.

## Conflict of Interest

The authors declare no conflict of interest.

## Data Availability Statement

The data that support the findings of this study are available in the supplementary material of this article.

**Keywords:** BODIPYs · chirality · circularly polarised luminescence · dissymmetry factor · naphthalene · near infrared luminescence

- [1] a) Y. Chen, J. Gao, X. Yang, *Adv. Opt. Mater.* **2019**, *7*, 1801467; b) D. Zhao, H. He, X. Gu, L. Guo, K. S. Wong, J. W. Y. Lam, B. Z. Tang, *Adv. Opt. Mater.* **2016**, *4*, 534–539; c) M. Schadt, *Ann. Rev. Mater. Sci.* **1997**, *27*, 305–379; d) M. C. Heffern, L. M. Matosziuk, T. J. Meade, *Chem. Rev.* **2014**, *114*, 4496–4539; e) C.-M. Jan, Y.-H. Lee, K.-C. Wu, C.-K. Lee, *Opt. Express* **2011**, *19*, 5431–5441; f) C.-J. Yu, C.-E. Lin, L.-P. Yu, C. Chou, *Appl. Opt.* **2009**, *48*, 758–764.
- [2] a) L. E. MacKenzie, R. Pal, *Nature Rev. Chem.* **2021**, *5*, 109–124; b) C. Zhang, Z. S. Li, X. Y. Dong, Y. Y. Niu, S. Q. Zang, *Adv. Mater.* **2022**, *34*, 2109496; c) H. Li, H. Li, W. Wang, Y. Tao, S. Wang, Q. Yang, Y. Jiang, C. Zheng, W. Huang, R. Chen, *Angew. Chem. Int. Ed.* **2020**, *59*, 4756–4762; *Angew. Chem.* **2020**, *132*, 4786–4792; d) H. Zheng, W. Li, W. Li, X. Wang, Z. Tang, S. X.-A. Zhang, Y. Xu, *Adv. Mater.* **2018**, *30*, 1705948.
- [3] a) J. Han, S. Guo, H. Lu, S. Liu, Q. Zhao, W. Huang, *Adv. Opt. Mater.* **2018**, *6*, 1800538; b) D.-W. Zhang, M. Li, C.-F. Chen, *Chem. Soc. Rev.* **2020**, *49*, 1331–1343; c) Y. Zhang, J. Li, Y. Quan, S. Ye, Y. Cheng, *Chem. Eur. J.* **2021**, *27*, 589–593; d) Y.-H. Kim, Y. Zhai, H. Lu, X. Pan, C. Xiao, E. A. Gaudling, P. Harvey Steven, J. Berry Joseph, V. Vardeny Zeev, M. Luther Joseph, C. Beard Matthew, *Science* **2021**, *371*, 1129–1133; e) M. Li, Y.-F. Wang, D. Zhang, L. Duan, C.-F. Chen, *Angew. Chem. Int. Ed.*

- 2020, 59, 3500–3504; *Angew. Chem.* **2020**, *132*, 3528–3532; f) G. Long, C. Jiang, R. Sabatini, Z. Yang, M. Wei, L. N. Quan, Q. Liang, A. Rasmita, M. Askerka, G. Walters, X. Gong, J. Xing, X. Wen, R. Quintero-Bermudez, H. Yuan, G. Xing, X. R. Wang, D. Song, O. Voznyy, M. Zhang, S. Hoogland, W. Gao, Q. Xiong, E. H. Sargent, *Nat. Photonics* **2018**, *12*, 528–533; g) D.-M. Lee, J.-W. Song, Y.-J. Lee, C.-J. Yu, J.-H. Kim, *Adv. Mater.* **2017**, *29*, 1700907; h) F. Zinna, U. Giovannella, L. D. Bari, *Adv. Mater.* **2015**, *27*, 1791–1795.
- [4] a) R. D. Richardson, M. G. J. Baud, C. E. Weston, H. S. Rzepa, M. K. Kuimova, M. J. Fuchter, *Chem. Sci.* **2015**, *6*, 3853–3862; b) D. Han, X. Yang, J. Han, J. Zhou, T. Jiao, P. Duan, *Nat. Commun.* **2020**, *11*, 5659; c) J. Yeom, B. Yeom, H. Chan, K. W. Smith, S. Dominguez-Medina, Joong H. Bahng, G. Zhao, W.-S. Chang, S.-J. Chang, A. Chuvilin, D. Melnikau, A. L. Rogach, P. Zhang, S. Link, P. Král, N. A. Kotov, *Nat. Mater.* **2015**, *14*, 66–72; d) T. Kawasaki, M. Sato, S. Ishiguro, T. Saito, Y. Morishita, I. Sato, H. Nishino, Y. Inoue, K. Soai, *J. Am. Chem. Soc.* **2005**, *127*, 3274–3275.
- [5] a) R. Carr, N. H. Evans, D. Parker, *Chem. Soc. Rev.* **2012**, *41*, 7673–7686; b) L. Zhang, H.-X. Wang, S. Li, M. Liu, *Chem. Soc. Rev.* **2020**, *49*, 9095–9120; c) Q. Cheng, A. Hao, P. Xing, *Nat. Commun.* **2021**, *12*, 6320; d) Z. Han, K. Wang, Y. Guo, W. Chen, J. Zhang, X. Zhang, G. Siligardi, S. Yang, Z. Zhou, P. Sun, W. Shi, P. Cheng, *Nat. Commun.* **2019**, *10*, 5117; e) D. Yang, J. Han, Y. Sang, T. Zhao, M. Liu, P. Duan, *J. Am. Chem. Soc.* **2021**, *143*, 13259–13265; f) H. Nian, L. Cheng, L. Wang, H. Zhang, P. Wang, Y. Li, L. Cao, *Angew. Chem. Int. Ed.* **2021**, *60*, 15354–15358; g) Y. Imai, Y. Nakano, T. Kawai, J. Yuasa, *Angew. Chem. Int. Ed.* **2018**, *57*, 8973–8978; *Angew. Chem.* **2018**, *130*, 9111–9116.
- [6] L. Arrico, L. Di Bari, F. Zinna, *Chem. Eur. J.* **2021**, *27*, 2920–2934.
- [7] a) *Circularly Polarized Luminescence of Isolated Small Organic Molecules* (Ed.: T. Mori), Springer Singapore, Singapore, **2020**; b) E. M. Sánchez-Carnerero, A. R. Agarrabeitia, F. Moreno, B. L. Maroto, G. Muller, M. J. Ortiz, S. De La Moya, *Chem. Eur. J.* **2015**, *21*, 13488–13500; c) M. Hasegawa, Y. Nojima, Y. Mazaki, *ChemPhotoChem* **2021**, *5*, 1042–1058; d) J.-L. Ma, Q. Peng, C.-H. Zhao, *Chem. Eur. J.* **2019**, *25*, 15441–15454; e) N. Chen, B. Yan, *Molecules* **2018**, *23*, 3376.
- [8] A. N. Bashkatov, E. A. Genina, V. I. Kochubey, V. V. Tuchin, *J. Phys. D* **2005**, *38*, 2543–2555.
- [9] J. Feng, L. Fu, H. Geng, W. Jiang, Z. Wang, *Chem. Commun.* **2020**, *56*, 912–915.
- [10] J. Jiménez, C. Díaz-Norambuena, S. Serrano, S. C. Ma, F. Moreno, B. L. Maroto, J. Bañuelos, G. Muller, S. De La Moya, *Chem. Commun.* **2021**, *57*, 5750–5753.
- [11] R. B. Alnoman, S. Rihn, D. C. O'Connor, F. A. Black, B. Costello, P. G. Waddell, W. Clegg, R. D. Peacock, W. Herrebout, J. G. Knight, M. J. Hall, *Chem. Eur. J.* **2016**, *22*, 93–96.
- [12] Y. Nakai, T. Mori, Y. Inoue, *J. Phys. Chem. A* **2012**, *116*, 7372–7385.
- [13] N. C. Bruno, M. T. Tudge, S. L. Buchwald, *Chem. Sci.* **2013**, *4*, 916–920.
- [14] N. Algoazy, J. G. Knight, P. G. Waddell, R. Aerts, W. Herrebout, H. H. T. Al-Sharif, J. K. G. Karlsson, A. Harriman, *Chem. Eur. J.* **2021**, *27*, 5246–5258.
- [15] M. Ponce-Vargas, C. Azarias, D. Jacquemin, B. Le Guennic, *J. Phys. Chem. B* **2017**, *121*, 10850–10858.
- [16] R. Sens, K. H. Drexhage, *J. Lumin.* **1981**, *24–25*, 709–712.
- [17] M. Head-Gordon, R. J. Rico, M. Oumi, T. J. Lee, *Chem. Phys. Lett.* **1994**, *219*, 21–29.
- [18] F. Weigend, R. Ahlrichs, *Phys. Chem. Chem. Phys.* **2005**, *7*, 3297–3305.
- [19] F. Neese, *WIREs Comput. Mol. Sci.* **2012**, *2*, 73–78.
- [20] L. Frédéric, A. Desmarchelier, R. Plais, L. Lavnevich, G. Muller, C. Villafuerte, G. Clavier, E. Quesnel, B. Racine, S. Meunier-Della-Gatta, J.-P. Dognon, P. Thuéry, J. Crassous, L. Favereau, G. Pieters, *Adv. Funct. Mater.* **2020**, *30*, 2004838.
- [21] P. Stachelek, L. MacKenzie, D. Parker, R. Pal, *Nat. Commun.* **2022**, *13*, 553.

---

Manuscript received: April 1, 2022

Revised manuscript received: May 27, 2022

Accepted manuscript online: May 30, 2022

Version of record online: June 30, 2022